e-ISSN 2320 –7876 www.ijfans.org
Vol.11, Iss.9, Dec 2022

Research Paper
Original article

Hydrothermal Synthesis and Characterization Of Tb_x $Pb_{1-X}Te$ Nanomaterials: Physical and Optical Properties

Chandrakumari. M, Dr. K. Rajendran
Bharath Institute of Higher Education and Research

Address for Correspondence
Chandrakumari. M
Bharath Institute of Higher Education And Research
Mail Id: kumari_ravi2006@yahoo.co.in

Abstract

The photovoltaic cells are very important due to their use as an alternate source of electricity. The first generation of photovoltaic cells is based on a single p-n junction of a crystalline-Si, exhibiting a power conversion efficiency of 15-20%. The poor absorbing properties of the crystalline Si and its high production cost have led to the use other various materials for photovoltaic technologies. The binary IV-VI compounds are the oldest known semiconducting materials used as photovoltaic materials and the most prominent representatives such as PbS, PbSe and PbTe, have been used for more than 100 years for electric and optoelectronic device applications. The first reported solid-state diode has been made from single crystal PbS in 1874 by Ferdinand Braun [1] and its rectifying properties have been exploited in the early radio receivers. The IV-VI compounds present specific electronic and transport properties, such as narrow band gaps, low resistivities, large carrier mobilities and positive temperature coefficients [2,3]. The phase transformation in the system GeSe-GeTe has been studied by Muir and Beato [16]. They have observed that a rhombohedral-cubic transformation occurs at 370 ± 10°C in alloys based on the GeTe structure and with composition in the range 0–55 mol% GeSe. The temperature and composition dependence of lattice parameters also have been determined for these alloys. Bhatia et al [17] have observed the first order transition in single crystals GeSe near 6 GPa.

INTRODUCTION

The transverse and longitudinal optical frequencies, the dielectric constant and the effective charges for the A^4 B^6 type family of the semiconducting compounds, namely, GeTe, SnTe

and PbTe have been presented by Zein et al. [21] using the density functional method with the use of the norm-conserving "first-principles" pseudopotentials. The electronic structure of the narrow gap IV-VI semiconducting compounds, namely, GeTe, SnTe and PbTe have been investigated by Ravindran and Asokamani [22] by employing the LMTO method. They also predicted that the electronic contribution arising from Te atom plays a dominant role in promoting superconductivity and s and p→d electron transfer is found to be responsible for the pressure induced superconductivity in these compounds. Lebedev and Sluchinskaya [23] have reported the low-temperature phase transitions in some quaternary solid solutions of IV-VI semiconductors. They have used electrical and X-ray methods on samples $PbS_xSe_yTe_{1-x-y}$, $Pb_{1-x}Sn_xTe_{1-y}Se_y$ and $Pb_{1-x}Sn_xTe_{1-y}S_y$. They concluded that the phase transitions in these solid solutions were associated with off-centre S and Sn ions. An “in-situ” X-ray diffraction study of the GeTe under shear deformation and nonhydrostatic pressure conditions has been performed by Serebryanaya et al [24]. They predicted that the structure changes from NaCl to GeS and further to CsCl types at 19.2 and 38 GPa respectively. Maclean et al [25] have carried out high pressure angle dispersive X-ray powder diffraction studies on IV-VI semiconductors using image plate detection. They suggested that the high-pressure intermediate phase for lead chalcogenide is monoclinic, as opposed to previously reported orthorhombic structure. Using a combination of high-resolution X-ray powder diffraction, Raman scattering, and ab-initio simulation, Hsueh et al. [26] presented the structural and vibrational properties of the prototypical layered semiconductor GeS. They observed GeS has no structural phase transition up to at least 94 kbar. High pressure electrical resistivity on cubic $SnTe_{1-x}Se_x$ has been reported by Ariponnammal et al [27]. They observed that the resistivity decreases gradually with the increase of pressure and then reaches saturation and the transition pressure decreases with the decrease of selenium concentration. Structural and electrical properties of GeSe and GeTe at high pressure have been reported by Onodera et al [28] using a combination of X-ray diffraction measurements, a diamond-anvil cell, and electrical-resistance measurements by employing an octahedral-anvil press. They have revealed that GeSe remains in the orthorhombic structure to at least 82 GPa, whereas GeTe transforms from the rhombohedral structure to the NaCl-type phase (GeTe-II) at 3 GPa and into another high-pressure phase (GeTe-III) at 18 GPa. Neutron scattering experiments were performed by Raty et al [29] on the liquid phases of a series of IV–VI compounds (GeS, GeSe, GeTe, SnS, SnSe and SnTe). They showed that the evolution of the local order was correlated with the conductivity measurements. Schwarzl et al [30] investigated the plasma

etching of IV-VI nanostructures using a CH_4/H_2 gas mixture. They predicted that etch rate decreases with the energy band gap. Furthermore, they also investigated the IV-VI quantum wires with vertical side walls by a combination of laser holography and CH_4/H_2/Ar plasma etching. The three-dimensional ordering of the PbSe dots in a trigonal lattice with a fcc-like ABCABC vertical stacking sequence have been showed by Springholz et al [31] using self-organization of PbSe islands in epitaxial $PbSe/Pb_{1-x}Eu_xTe$ superlattices. Using X-ray diffraction they predicted that reciprocal space maps, the interlayer correlation direction of the PbSe dots were to be inclined by 400 with respect to the [111] surface normal. Peak profile measurements of ordered regions showed coherence length of order of 300±100 nm in the lateral, and of 530±50 nm in the vertical direction. The structure and dynamics of semiconducting liquid GeSe using ab-initio molecular-dynamics simulations have been investigated by Raty et al [32]. They showed that the Peierls distortion reenters GeSe in the melt phase. They also examined the distance histograms and concluded that there is one Ge-Ge defective bond in GeSe3 unit.

COMPUTATIONAL & EXPERIMENTAL DETAILS:

INTRODUCTION

In this chapter we explained the computational and experimental details of lead chalcogenides. The theoretical study of structural, optical and electronics properties of lead chalcogenides PbX (X=S, Se and Te) were performed with CRYSTAL [1] code which is based on ab-initio calculations of ground state energy, energy gradient, electronic wave functions and properties of periodic systems. The researchers of the Theoretical Chemistry group in Torino (Italy) and the Computational materials sciences group in CLRC (Daresbury, UK) developed this code. With the use of this package, ab-initio calculations of ground state properties of the periodic systems in 3D (crystals), 2D (slabs), 1D (polymers) and 0D (molecules) can be performed.

At the present time, electronic band structure calculations are being widely used by theoretician and experimentalists to explore the electronic, optical and magnetic properties, etc. of various compounds. There are two fundamental schemes to study the structural, electronic and other important properties of compounds: Hartree-Fock (HF) approximation and density functional theory (DFT). For the sake of completion, a brief discussion of HF and DF theory are described below.

e-ISSN 2320 –7876 www.ijfans.org
Vol.11, Iss.9, Dec 2022

Research Paper

HARTREE- FOCK (HF) THEORY

HF theory was discovered by D.R.Hartree in 1927. It is an iterative method to find out the ground state energy and the wave function. In this theory, the whole information of system is confined in the wave function of that system. This theory is mainly used in Quantum Mechanics and Atomic and molecular Physics to solve the many body problems. HF theory is an ab-initio method for solving the many-body Schrödinger equation i.e.

$$H\psi_i\ (1,2,...N) = E_i\psi_i\ (1,2,...N)$$

where H is the Hamiltonian of a quantum mechanical system composed of N particles, ψ_i is its i^{th} wave-function and E_i is the energy eigen value of the i^{th} state. The coordinates (1, 2, ... N) are particle coordinates and are usually associated with a spin and a position coordinate. For electronic systems the Hamiltonian (within non-relativistic approximations) for an N-electron system is:

$$H = -\frac{1}{2}\sum_{i=1}^{N}\nabla_i^2 + \sum_{i>j}^{N}\frac{1}{|\mathbf{r}_i - \mathbf{r}_j|} + \sum_{i=1}^{N}\upsilon(\mathbf{r}_i)$$

where the first, second and third terms of right-hand side represent the electron kinetic energy, the electron-electron Coulomb interactions and the coulomb potential generated by the nuclei. It is assumed that the nuclei are effectively stationary with respect to electron motion (Born-Oppenheimer approximation). The HF method attempts to transform the full N-body equation into N singlebody equations. One can determine the ground state of the Hamiltonian, H, quantum mechanically by means of the variational principle for the normalised eigen function Ψ (1, 2, ……..N) :

$$\langle\Psi|H|\Psi\rangle = \sum_{s_1}\sum_{s_2}\cdots\sum_{s_N}\int\Psi^*(1,2,...,N)H\Psi(1,2,...,N)d\mathbf{r}_1\,d\mathbf{r}_2\ldots d\mathbf{r}_N = \text{minimum} = E_0$$

where, i s is the spin direction of the i^{th} electron.

DENSITY FUNCTIONAL THEORY (DFT)

DFT is a quantum mechanical modelling method which is widely used to investigate ground state properties of different materials. With the use of DFT, the

properties of many-electron system can be determined by using functional i.e., functions of another function, which is spatially dependent electron density in the case of DFT. It is the most versatile method of electronic structure calculations in condensed matter physics.

The concept of DFT is based on two remarkable Hohenberg- Kohn theorems.

The first Hohenberg-Kohn theorem [2] states that the ground state energy of a system of electrons is a unique functional of ground state density:

$$E_{GS} = E[n_{GS}]$$

Not only ground state energy of a system but all properties of the system including excited state properties are exact functionals of the ground state density because there is one-to-one mapping between the ground state density and the external potential. If the ground state density is known then, in principle, the external potential is known and the external potential can solve the manyelectron Schrodinger equation, hence everything about the system can be known.

The internal electronic energy F, of a system in its ground state can be expressed as

$$F = E\text{-}V_{ext}$$

Where V_{ext} is the external potential energy, given by

$$V_{ext} = \int n(\mathbf{r}) v_{ext}(\mathbf{r}) d\mathbf{r}$$

Since E and V_{ext} are functions of the density, it follows that F is also functional of the density. Hence it can be written

$$E_{(v,N)}[n] = F[n] + \int n_0(\mathbf{r}) v(\mathbf{r}) d\mathbf{r}$$

The second Hohenberg-Kohn theorem states that if N interacting electrons move in an external potential $v_{ext}(r)$, the ground state electron density no (r) minimizes the functional

$$E[n] = F[n] + \int n(\mathbf{r}) v(\mathbf{r}) d\mathbf{r}$$

where, F is a universal functional of n and the minimum value of the functional E is E_0 (the exact ground state electronic energy).

e-ISSN 2320 –7876 www.ijfans.org
Vol.11, Iss.9, Dec 2022

Kohn and Sham [3] derived few differential equations enabling the ground state density n_0 (r) to be determined. Kohn-Sham equation is defined by a local effective external potential in which the non-interacting particles move, known as Kohn-Sham potential. This potential is denoted by v_{eff} (r). The Hamiltonian of the non-interacting system is given as:

$$\hat{H}_s = \sum_i^N \frac{-\hbar^2}{2m}\nabla_i^2 + \sum_i^N v_{eff}(\mathbf{r}_i)$$

The wave function describing this system is a Slater determinant constructed from a set of orbitals that are the lowest energy solutions to

$$\left[\frac{-\hbar^2}{2m}\nabla_i^2 + v_{eff}(\mathbf{r})\right]\phi_i(r) = \varepsilon_i\phi_i(r)$$

This equation is typically representation of the Kohn-Sham equations. Here, ε_i is the orbital energy of the corresponding Kohn-Sham orbitals, ϕ_i , and the electron density distribution is given by:

$$n(\mathbf{r}) = \sum_{i=1}^{N} |\phi_i(r)|^2$$

The total energy of a system is expressed as a functional of the charge density as

$$E[n] = T_s[n] + \int n(\mathrm{r}) v_{ext}(\mathrm{r}) dr + V_H[n] + E_{xc}[n]$$

where, T_s [n] is the Kohn-Sham kinetic energy which can be expressed in terms of the Kohn-Sham orbitals as

$$T_s[n] = \sum_{i=1}^{N} \int dr \phi_i^*(r)\left(\frac{-\hbar^2}{2m}\nabla^2\right)\phi_i(r)$$

V_{ext} (r) is the external potential acting on interacting system, V_H is the Hartee energy which is expressed as

$$V_H = \frac{e^2}{2}\int dr \int dr' \frac{n(r)n(r')}{|r - r'|}$$

e-ISSN 2320 –7876 www.ijfans.org
Vol.11, Iss.9, Dec 2022

and E_{xc} [n] is the exchange-correlation energy. The Kohn-Sham equations can be originated by varying the total energy expression with respect to a set of orbitals to obtain the Kohn-Sham potential as

$$v_{eff}(\mathbf{r}) = v_{ext}(\mathbf{r}) + \int \frac{n(\mathbf{r}')}{|\mathbf{r}-\mathbf{r}'|} d\mathbf{r}' + v_{xc}(\mathbf{r})$$

With the exchange-correlation potential is defined as

$$v_{xc}(\mathbf{r}) = \frac{\delta E_{xc}[n]}{\delta n(\mathbf{r})}$$

The above equations provide a theoretically exact method for finding the ground state energy of an interacting system provided that exchange-correlation energy E_{xc} is known.

EXCHANGE-CORRELATION POTENTIAL

The investigation of accurate and suitable exchange-correlation energy E_{xc} is the greatest challenge in the density functional theory. The approximations can be divided into two classes. Local Density Approximation (LDA) Local Density Approximation (LDA) is that class of approximations to the exchange-correlation energy functional that depends only on the value of the electronic density at each point in space. Local approximations are derived from the homogeneous electron gas (HEG) model. In the local density approximation, the exchange and correlation energy is given

$$E_{xc}^{LDA}[n] = \int n(\mathbf{r}) \varepsilon_{xc}(n) d\mathbf{r}$$

where, n is the electronic density, ε_{xc} is the exchange and correlation energy per particle. The function ε_{xc} can be divided into two parts as

$$\varepsilon_{xc}(n) = \varepsilon_x(n) + \varepsilon_c(n)$$

where ε (n) and ε_c(n) are exchange and correlation contributions respectively. Initially, the exchange contribution was given by the Dirac exchange energy functional [4]:

e-ISSN 2320 –7876 www.ijfans.org
Vol.11, Iss.9, Dec 2022

Research Paper

$$\varepsilon_x(n) = -\frac{3}{4}\left(\frac{3}{\pi}\right)^{1/3} n(\mathbf{r})^{1/3}$$

Accurate values of correlation part ε_c (ρ) are available in the literature [5,6]. The von Barth-Hedin [vBH] is the most popular LDA scheme in the solid-state applications.

GENERALISED GRADIENT APPROXIMATION (GGA)

LDA is suitable only for those systems which have uniform electron density distribution. LDA does not include the effects of inhomogeneity of the electron density distribution. The exchange- correlation energy for the systems, which have non-uniform charge densities, can be derived by GGA. Hence, in GGA, an improvement is made by considering the dependence of exchange correlation functional on the electron density and on the gradient of the electron density distribution at the point of consideration. Mathematically, the exchange-correlation energy, in the generalized gradient approximation, can be written as

$$E_{xc}^{GGA} = E_{xc}\left[\mathrm{n(r)}, \nabla n(\mathrm{r})\right]$$

There are several proposed GGA schemes. One of these is due to Perdew and Wang [7]. The hybrid functional like B3PW and B3LYP can be computed using the Becke exchange [8] combined with the Perdew-Wang GGA correlation scheme.

GROUND STATE PROPERTIES

Various ground state properties can be calculated using the CRYSTAL code as follows: Structural parameters In order to calculate the structural parameters like lattice parameter (a), bulk modulus (B_0) and its pressure derivatives (B_0'), the total energy versus volume dependency for different crystal structures is to be determined. Subsequently, these values can be fitted to the Birch Murnaghan equation of state [9,10]

$$E(V) = E_0 + \frac{9V_0B_0}{16}\left\{\left[\left(\frac{V_0}{V}\right)^{2/3} - 1\right]^3 B_0^{'} + \left[\left(\frac{V_0}{V}\right)^{2/3} - 1\right]^2 \left[6 - 4\left(\frac{V_0}{V}\right)^{2/3}\right]\right\}$$

e-ISSN 2320 –7876 www.ijfans.org
Vol.11, Iss.9, Dec 2022

where, E_0 is minimum energy per formula unit in the equilibrium, V_0 is corresponding volume, B_0 is the bulk modulus, and B_0' is pressure derivative of the bulk modulus. The pressure versus volume data for the compounds can be calculated from the third order Birch-Murnaghan [9,10] isothermal equation of state relating pressure and volume as follows:

$$P(V)=\frac{3B_0}{2}\left[\left(\frac{V_0}{V}\right)^{7/3}-\left(\frac{V_0}{V}\right)^{5/3}\right]\left\{1+\frac{3}{4}\left(B_0^{'}-4\right)\left[\left(\frac{V_0}{V}\right)^{2/3}-1\right]\right\}$$

To determine the transition pressure, the Gibbs free energy

($G = E_o + PV - TS$) is used. At zero temperature the thermodynamically stable phase is that one which has lowest enthalpy, $H = E + PV$, at a given pressure. The variation in the enthalpy (H) of compound with pressure (P) is to be plotted in stable and other phases. When the enthalpy of the lower pressure phase coincides with that of other phase, the transformation from one phase to another phase occurs.

OPTICAL PROPERTIES

The dielectric constant of a compound can be determined by the finite field approach which is embodied in CRYSTAL06 code. To evaluate the dielectric constants for compounds, following steps are to be followed:

a) Evaluation of the perturbed total energy (TE) and the electron density of the system by running the calculations (keyword FIELD).

b) Determination of dielectric tensor element by running the properties calculation (keyword DIEL).

ELECTRONIC PROPERTIES

To study the electronic properties of different compounds, the calculations of band structure and densities of states (DOS) of compounds are to be made through CRYSTAL06 code. The keyword BAND is used to compute the band structures. For the band structure, the input requires:

To study the electronic properties of different compounds, the calculations of band structure and densities of states (DOS) of compounds are to be made through CRYSTAL06 code. The keyword BAND is used to compute the band structures. For the band structure, the input requires:

a) The path of the Brillouin zone in reciprocal space.

b) Number and range of energy bands.

c) Number of k-points in the Brillouin zone.

To calculate the DOS, the keyword NEWK is used. For DOS, the input requires:

a) The energy range of DOS

b) The degree of polynomials

STRUCTURAL AND ELECTRONIC PROPERTIES OF DOPED LEAD-CHALCOGENIDES

The lead chalcogenides (PbX, X=S, Se and Te) are a special class of IV-VI narrow band gap (0.2-0.4 eV) semiconductors. Due to its unique structural and electronics properties, these materials are of great interest of research from past few decades. Many experimental and theoretical studies have been performed on their structural and electronic properties [1-6].

All these theoretical calculations identified a direct band gap at L point of Brillouin zone (BZ) for all lead chalcogenides. These materials are stable in the rocksalt structure at ambient temperature and pressure.

It is well known that, by introducing foreign atom into a semiconductor, structural and electronic properties can be changed. The doping process can significantly affect the physical properties of lead chalcogenides, and it provides an easy way of changing the grain size and thus, its emission and absorption wavelength, or optical band gap of these materials.

To learn more about the nature of these materials, few experimental and theoretical studies were performed on structural and electronic properties of doped lead chalcogenides.

In the present work, the structural and electronic properties of ternary alloys $PbS_{1-x}Se_x$, $PbS_{1-x}Te_x$ and $PbSe_{1-x}Te_x$ (x=0.0, 0.25, 0.50, 0.75, 1.0) have been reported using LCAO method. These properties are studied in terms of lattice constant, bulk modulus, pressure derivative of bulk modulus and energy band gap. Variation in lattice constant, bulk modulus and in energy band gap as a function of concentration i.e. x for $PbS_{1-x}Se_x$, $PbS_{1-x}Te_x$ and $PbSe_{1-x}Te_x$ alloys are estimated. An outline of this chapter is as follows: A brief description of computational details is given in Section 4.2 and the results are discussed in Section 4.3. The last Section 4.4 summarizes the results of this investigation.

e-ISSN 2320 –7876 www.ijfans.org
Vol.11, Iss.9, Dec 2022

Research Paper

COMPUTATIONAL DETAILS

The ab-initio LCAO method embodied in CRYSTAL06 code [16] have been used to study the structural and electronic properties of $PbS_{1-x}Se_x$, $PbS_{1-x}Te_x$ and $PbSe_{1-x}Te_x$ alloys. In this method, each crystalline orbital $\psi i(r,k)$ is a linear combination of Bloch functions $\varphi\mu(r,k)$. The Bloch functions are defined in terms of local functions $\varphi\mu(r)$, normally referred as atomic orbitals. There are a few fundamental schemes exist for constructing the Hamiltonian for the periodic solids, in which HF approximation [17] and the DFT [18] are the well-known approaches among these schemes. Under the DFT, a number of functional exist to treat exchange and correlation. In the present work, the local functions for Pb, S, Se and Te were constructed from the Gaussian type basis sets [19]. The Kohn-Sham Hamiltonian was constructed while considering the exchange scheme of Becke [20] and correlation scheme of PBE [21].

STRUCTURAL PROPERTIES

The ground state properties such as the lattice constants (a), bulk modulus (B), pressure derivative of bulk modulus (B') were computed by fitting the total energy versus volume according to the third order BirchMurnaghan equation of state [22,23]. The calculated lattice constants and bulk modulus for B1 phase of the binary compounds (PbS, PbSe and PbTe) and their alloys

($PbS_{1-x}Se_x$, $PbS_{1-x}Te_x$ and $PbSe_{1-x}Te_x$) are listed in Tables 4.1-4.3, which also contain the previous theoretical and experimental results. The calculated structural parameters are in good agreement with the previous results.

To the best of my knowledge, no experimental data are available for structural parameters of the ternary alloys ($PbS_{1-x}Se_x$, $PbS_{1-x}Te_x$ and $PbSe_{1-x}Te_x$). Hence, our calculated results can serve as a prediction for future research. Figures 4.1(a)-(c) show the variation of the calculated lattice constant versus concentration for the alloys $PbS_{1-x}Se_x$, $PbS_{1-x}Te_x$ and $PbSe_{1-x}Te_x$) respectively. From these Figures, it is clear that the values of calculated lattice constant vary with the concentration of doping in the similar trend with the values of Vegard' s law [24] with small deviation. Figures 4.2(a)-(c) show the variation of the calculated bulk modulus versus concentration for the alloys $PbS_{1-x}Se_x$, $PbS_{1-x}Te_x$ and $PbSe_{1-x}Te_x$ respectively.

ELECTRONIC PROPERTIES

e-ISSN 2320 –7876 www.ijfans.org
Vol.11, Iss.9, Dec 2022

In order to compute the energy band gap, calculated equilibrium lattice constant are used. The electronic band structures for B1 phase of the ternary alloys $PbS_{1-x}Se_x$, $PbS_{1-x}Te_x$ and $PbSe_{1-x}Te_x$ (x=0.25, 0.50 and 0.75) are shown in Figures 4.3-4.11 respectively. In the ternary alloys $PbS_{1-x}Se_x$, $PbS_{1-x}Te_x$ and $PbSe_{1-x}Te_x$ with concentration of doping x=0.25 and 0.75, the valence band maximum (VBM) and conduction band minimum (CBM) occur at the L point of Brillouin zone (BZ) but for x=0.50, direct band gaps are observed along the highly symmetric direction (i.e Γ). The calculated and available previous results of the energy band gaps are given in Table 4.4.

Table 4.1

Calculated lattice parameter (a), bulk modulus (B_0) and its pressure derivatives (B_0 ') for $PbS_{1-x}Se_x$ (x=0, 0.25, 0.5, 0.75 and 1.0).

e-ISSN 2320 –7876 www.ijfans.org
Vol.11, Iss.9, Dec 2022

Research Paper

		x= 0	x = 0.25	x = 0.50	x = 0.75	x= 1
a (Å)						
	Present	5.89	5.92	6.028	6.04	6.08
	Vegards Law	5.89	5.93	5.98	6.03	6.08
	Experiment	5.940[1], 5.936[2], 5.929[3]	-	-	-	6.133[1], 6.124[2], 6.117[3]
	Other Calculations	6.000[4], 6.006[5], 6.012[6], 6.012[14], 6.010[15]	6.069[14], 6.073[15]	6.122[14], 6.128[15]	6.174[14], 6.179[15]	6.211[4], 6.214[5], 6.226[6], 6.565[14], 6.210[15]
B_0 (GPa)						
	Present	67.9	67.6	67.2	67.1	66.9
	Experiment	62.8[2], 62.2[3]	-	-	-	54.1[2], 54.1[3]
	Other calculations	54.63[4], 56.0[5], 52[6], 53.3[14], 53.38[15]	50.8[14], 49.21[15]	49.7[14], 47.46[15]	48.2[14], 46.78[15]	48.27[4], 49.5[5], 44.5[6], 49.1[14], 49.18[15]
B_0'						
	Present	3.9	4.2	4.3	4.1	4
	Experiment	-	-	-	-	-
	Other calculations	4.10[4], 3.6[5]	-	-	-	4.35[4], 3.8[5]

Table 4.2

Calculated lattice parameter (a), bulk modulus (B_0) and its pressure derivatives (B_0 ') for $PbS_{1-x}Te_x$ (x=0, 0.25, 0.5,0.75 and 1.0)

e-ISSN 2320 –7876 www.ijfans.org
Vol.11, Iss.9, Dec 2022

		x= 0	x = 0.25	x = 0.50	x = 0.75	x= 1
a (Å)						
	Present	5.89	6.0	6.15	6.25	6.462
	Vegards Law	5.89	6.033	6.176	6.319	6.462
	Experiment	5.940[1], 5.936[2], 5.929[3]	-	-	-	6.458[1], 6.462[2], 6.443[3]
	Other calculations	6.000[4], 6.006[5], 6.012[6], 6.010[15]	6.188[15]	6.325[15]	6.450[15]	6.554[4], 6.566[5], 6.582[6], 6.560[15]
B_0 (GPa)						
	Present	67.9	63	57.5	53.4	49
	Experiment	62.8[2], 62.2[3]	-	-	-	39.8[2], 41.1[3]
	Other calculations	54.63[4], 56.0[5], 52[6], 53.384[15]	45.744[15]	44.368[15]	39.462[15]	39.95[4], 41.0[5], 37.5[6], 38.406[15]
B_0'						
	Present	3.9	4.1	4	3.9	4.1
	Experiment	-	-	-	-	-
	Other calculations	4.10[4], 3.6[5]	-	-	-	4.32[4], 4.6[5]

Table 4.3

e-ISSN 2320 –7876 www.ijfans.org
Vol.11, Iss.9, Dec 2022

Research Paper

Calculated lattice parameter (a), bulk modulus (B_0) and its pressure derivatives (B_0 ') for $PbSe_{1-x}Te_x$ (x=0, 0.25, 0.5, 0.75 and 1.0).

		x= 0	x = 0.25	x = 0.50	x = 0.75	x= 1
a (Å)						
	Present	6.08	6.25	6.35	6.36	6.462
	Vegards Law	6.08	6.175	6.271	6.366	6.462
	Experiment	6.133[1], 6.124[2], 6.117[3]	-	-	-	6.458 [1], 6.462[2], 6.443[3]
	Other calculations	6.211[4], 6.214[5], 6.226[6], 6.210[15]	6.320[15]	6.406[15]	6.487[15]	6.554[4], 6.566[5], 6.582[6], 6.560[15]
B_0 (GPa)						
	Present	66.9	60.3	57.8	52.5	49
	Experiment	54.1[2], 54.1[3]	-	-	-	39.8[2], 41.1[3]
	Other calculations	48.27[4], 49.5[5], 44.5[6], 49.187[15]	44.489[15]	41.101[15]	37.791[15]	39.95[4], 41.0[5], 37.5[6], 38.406[15]
B_0'						
	Present	4	4.3	3.9	4.2	3.8
	Experiment	-	-	-	-	-
	Other calculations	4.35[4], 3.8[5]	-	-	-	4.32[4], 4.6[5]

e-ISSN 2320 –7876 www.ijfans.org
Vol.11, Iss.9, Dec 2022

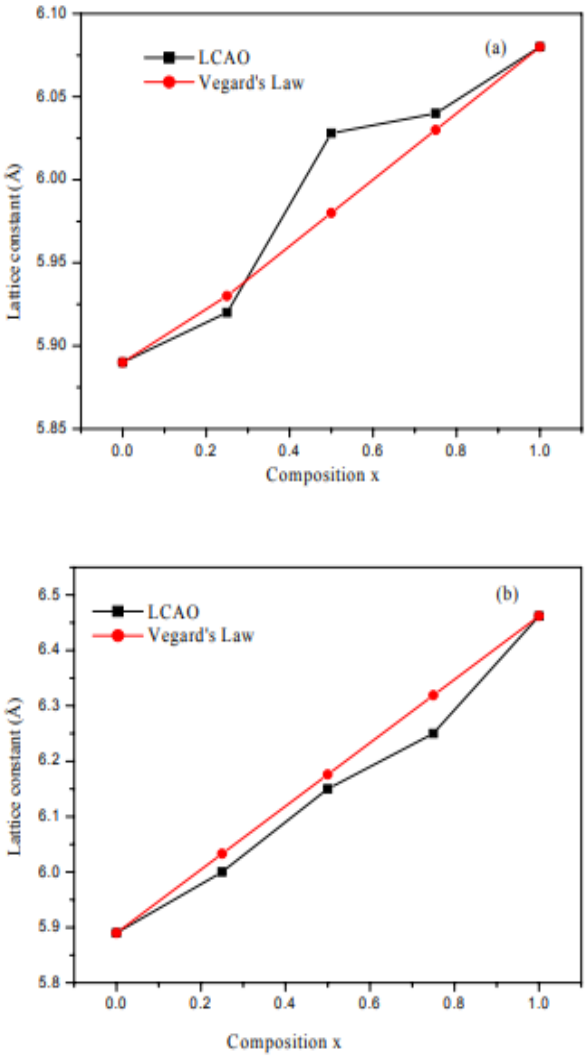

Figure 4.1 Calculated lattice constants as a function of composition for (a) $PbS_{1-x}Se_x$,(b) $PbS_{1-x}Te_x$ and (c) $PbSe_{1-x}Te_x$ alloys.

e-ISSN 2320 –7876 www.ijfans.org
Vol.11, Iss.9, Dec 2022

Research Paper

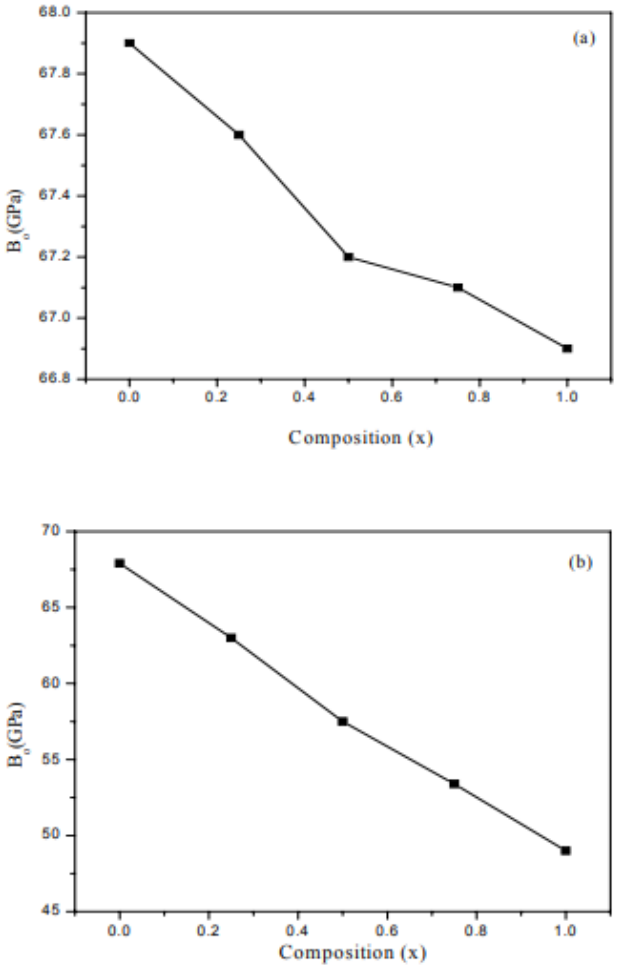

Figure 4.2 Calculated bulk modulus as a function of composition for (a) $PbS_{1-x}Se_x$,(b) $PbS_{1-x}Te_x$ and (c) $PbSe_{1-x}Te_x$ alloys.

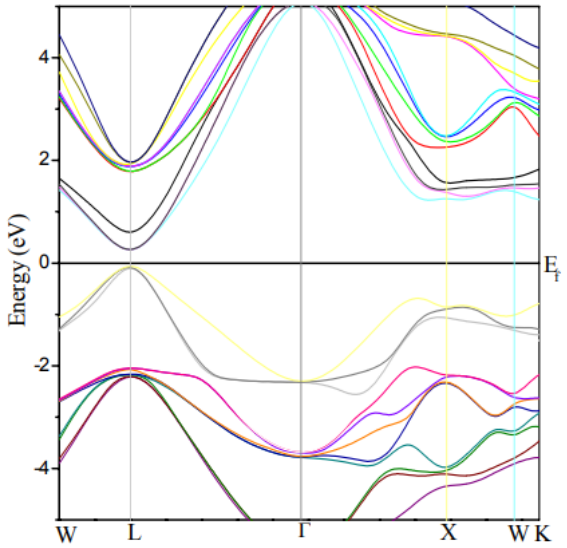

Figure 4.3 Energy band structure of B1 phase of PbS0.75Se0.25.

e-ISSN 2320 –7876 www.ijfans.org
Vol.11, Iss.9, Dec 2022

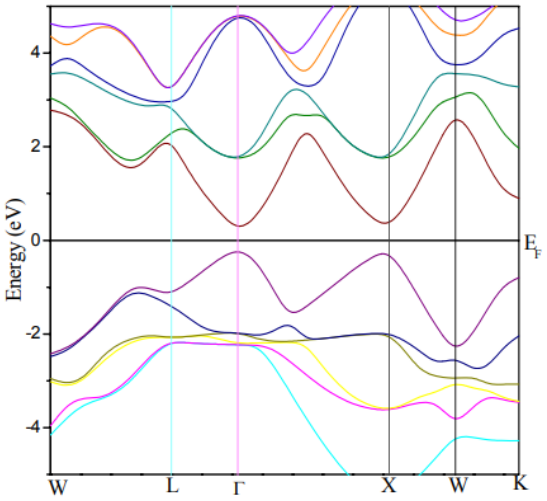

Figure 4.4 Energy band structure of B1 phase of PbS0.50Se0.50.

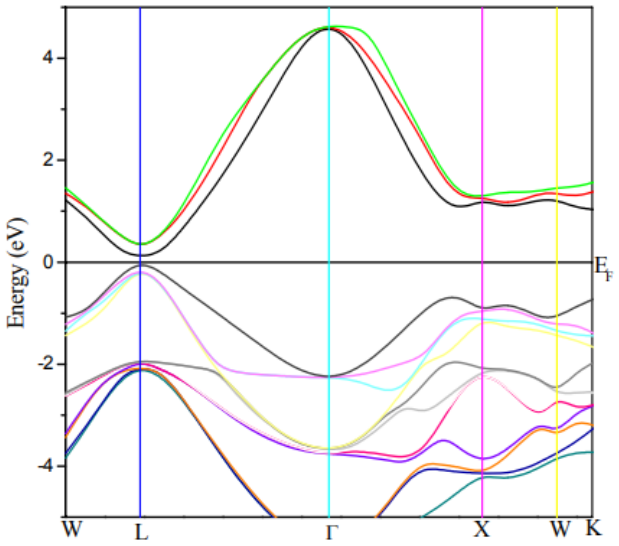

Figure 4.5 Energy band structure of B1 phase of PbS0.25Se0.75.

e-ISSN 2320 –7876 www.ijfans.org
Vol.11, Iss.9, Dec 2022

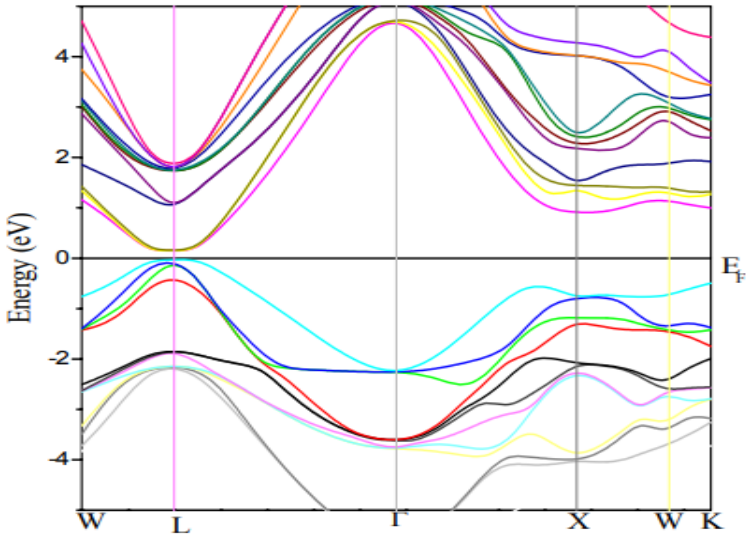

Figure 4.6 Energy band structure of B1 phase of PbS0.75Te0.25.

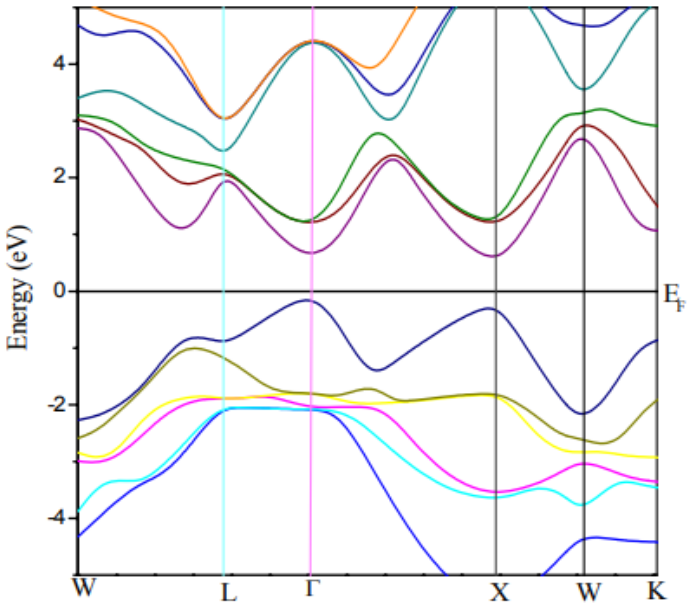

Figure 4.7 Energy band structure of B1 phase of PbS0.50Te0.50.

e-ISSN 2320 –7876 www.ijfans.org
Vol.11, Iss.9, Dec 2022

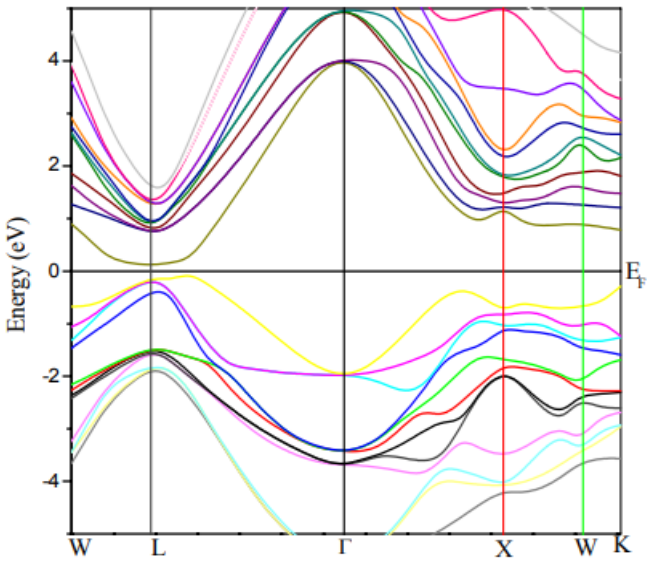

Figure 4.8 Energy band structure of B1 phase of PbS0.25Te0.75

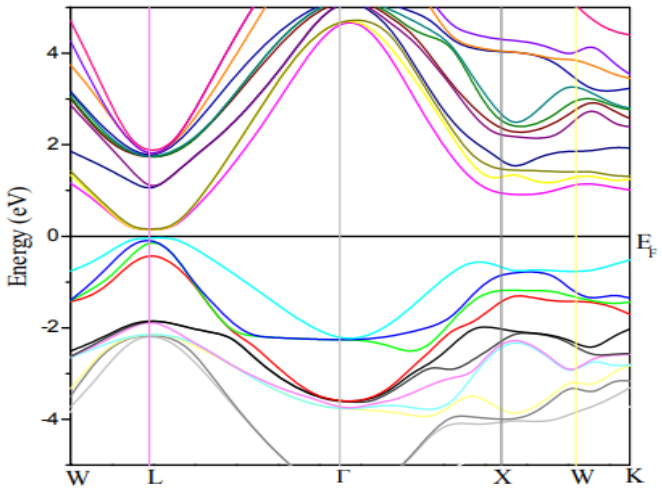

Figure 4.9 Energy band structure of B1 phase of PbSe0.75Te0.25.

e-ISSN 2320 –7876 www.ijfans.org
Vol.11, Iss.9, Dec 2022

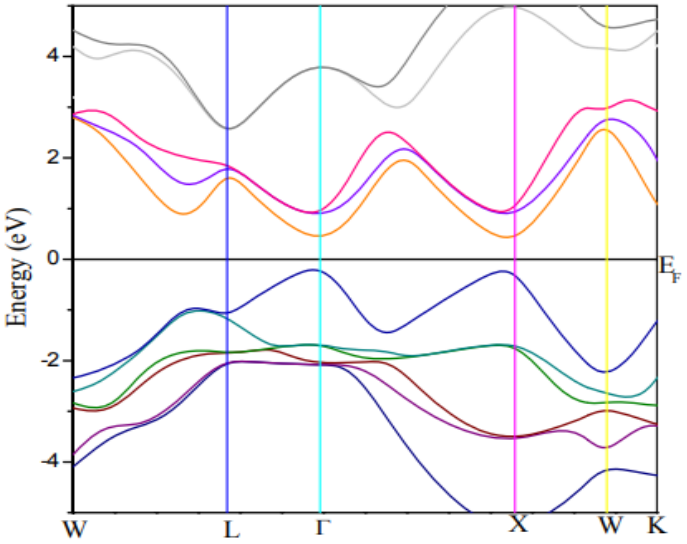

Figure 4.10 Energy band structure of B1 phase of PbSe0.50Te0.50.

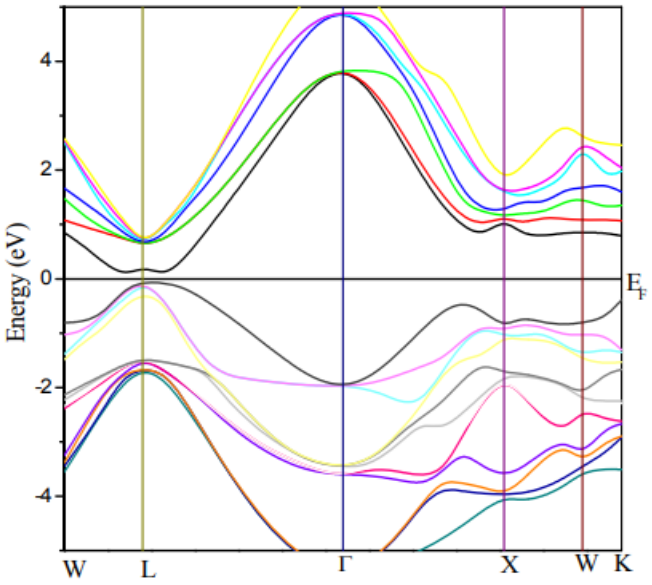

Figure 4.11 Energy band structure of B1 phase of PbSe0.25Te0.75.

Table 4.4

e-ISSN 2320 –7876 www.ijfans.org
Vol.11, Iss.9, Dec 2022

Energy band gap (in eV) for $PbS_{1-x}Se_x$, $PbS_{1-x}Te_x$ and $PbSe_{1-x}Te_x$ (x=0, 0.25, 0.5, 0.75 and 1.0).

		x= 0	x = 0.25	x = 0.50	x = 0.75	x= 1
$PbS_{1-x}Se_x$						
	Present	0.36	0.2	1.21	0.1	0.18
	Experiment	0.29[25]	-	-	-	0.17[25]
	Other Calculations	0.496[15], 0.26[26], 0.29[27], 0.380[28]	0.427[15], 0.340[28], 0.295[29]	0.342[15], 0.737[28], 0.730[28]	0.329[15]	0.425[15], 0.16[26], 0.17[27]
$PbS_{1-x}Te_x$						
	Present	0.36	0.11	1.20	0.2	0.26
	Experiment	0.29[25]	-	-	-	0.19[25]
	Other calculations	0.496[15], 0.26[26], 0.29[27]	0.256[15]	0.161[15]	0.136[15]	0.833[15], 0.17[26], 0.19[27]
$PbSe_{1-x}Te_x$						
	Present	0.18	0.13	1.18	0.23	0.26
	Experiment	0.17[25]	-	-	-	0.19[25]
	Other calculations	0.425[15], 0.16[26], 0.17[27]	0.329[15]	0.342[15]	0.427[15]	0.496[15] 0.17[26], 0.19[27]

e-ISSN 2320 –7876 www.ijfans.org
Vol.11, Iss.9, Dec 2022

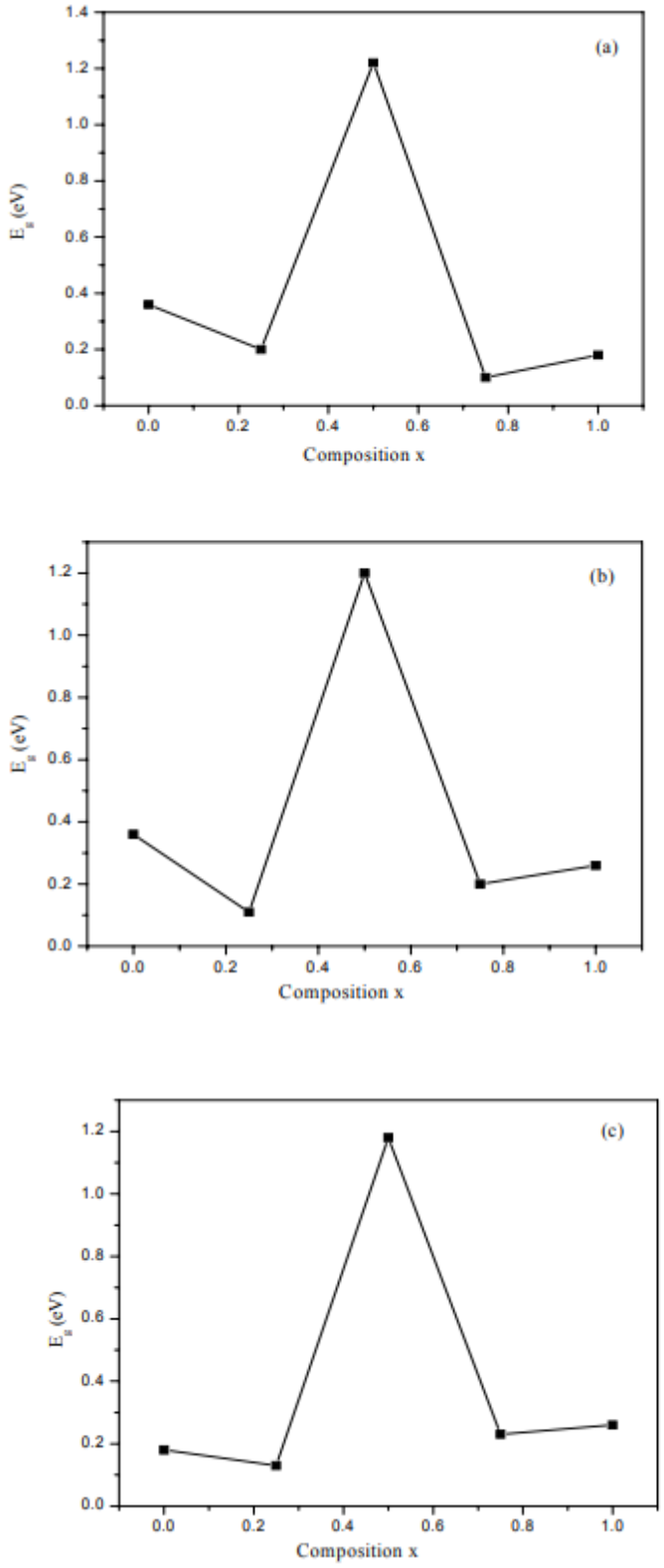

Figure 4.12 Calculated Energy band gap as a function of composition for (a) $PbS_{1-x}Se_x$,(b) $PbS_{1-x}Te_x$ and (c) $PbSe_{1-x}Te_x$ alloys.

For better visualizing, the variation of the energy band gap with the concentration of doping for the alloys $PbS_{1-x}Se_x$, $PbS_{1-x}Te_x$ and $PbSe_{1-x}Te_x$ is presented in Figure 4.12(a)-(c) respectively. The Figure 4.12(a)-(c) depict the energy band gap of the alloys $PbS_{1-x}Se_x$, $PbS_{1-x}Te_x$ and $PbSe_{1-x}Te_x$ vary in similar manner with concentration of doping.

CONCLUSIONS

Lead-chalcogenides are some promising semiconductor materials used for photovoltaics due to their fascinating properties like high carrier mobility, high dielectric constant and narrow band gap. These semiconductor materials crystallize in the rock salt structure at ambient conditions. These materials can also be used in non-linear optical devices and detectors because of their very unusual electronic, optical and structural properties. The lead chalcogenides PbX (with X=S, Se, Te) are of great importance for infrared detection and lasing devices and furthermore find applications as thermoelectric materials as window coatings and in solar-energy panels.

In the past decades, nanoscience and nanotechnology have been making significant progress, and their effects on every field have been acknowledged in the world. The nanomaterials have attracted enormous attention due to their size-dependent unique mechanical, physical and chemical properties. Among them, one dimensional semiconductor nanostructures (such as nanowires, nanorods and nanotubes) are promising candidates for technological nanoscale electronic, optoelectronic and photonic applications. Solution-based chemical synthesis of semiconductor nanostructures has allowed tremendous flexibility in crystal morphology. The inherent size dependence of the nanocrystal properties is the result of quantum confinement. Quantum size effect occurs when the nanostructures become smaller than a fundamental scale, which is determined by the exciton Bohr radius. IV-VI materials offer unique access to the regime of extreme quantum confinement because of their relatively large Bohr radii. Due to large Bohr radii, strong quantum confinement in IV-VI can be achieved in relatively large structures, consequently, band gap of IV-VI semiconductors can be easily tuned by changing their sizes, and hence these materials can be easily used in optoelectronic devices.

REFRENCES

[1] V.R. Saunders, R. Dovesi, C. Roetti, M. Causµa, N.M. Harrison, R. Orlando and C.M. Zicovich-Wilson, CRYSTAL06 User's manual (University of Torino, 2006).

[2] P. Hohenberg and W. Kohn, Inhomogeneous Electron Gas, Phys. Rev. 136 (1964) B864.

[3] W. Kohn and L. Sham, Self-Consistent Equations Including Exchange and Correlation Effects, Phys. Rev. 140 (1965) A1133.

[4] P.A.M. Dirac, Quantum Mechanics of Many-Electron Systems, Proc. R. Soc. A 123 (1929) 792.

[5] D.M. Ceperley and B.J. Alder, Ground State of the Electron Gas by a Stochastic Method, Phys. Rev. Lett. 45 (1980) 566.

[6] S.H. Vosko, L. Wilk and M. Nusair, Accurate spin-dependent electron liquid correlation energies for local spin density calculations: a critical analysis, Can. J. Phys. 58 (1980) 1200.

[7] J.P. Perdew and Y. Wang, Accurate and simple density functional for the electronic exchange energy: Generalized gradient approximation, Phys. Rev. B 33 (1986) 8800.

[8] A.D. Becke, Density-functional thermochemistry. III. The role of exact exchange, J. Chem. Phys. 98 (1993) 5648

[9] F. Brich, Finite elastic strain of cubic crystals, J. Geophys. Res. 83 (1978) 1257.

[10] J.P. Poirer, Introduction to the Physics of Earth’s Interior, Cambridge University Press, Cambridge, 27 (1992) 193.

[11] M.J. Cooper, Compton scattering and electron momentum determination, Rep. Prog. Phys. 48 (1985) 415.

[12] M.J. Cooper, P.E. Mijnarends, N. Shiotani, N. Sakai and A. Bansil, X-Ray Compton Scattering (Oxford: Oxford Publishing Press), (2004).

[13] www. Innerfidelity.com.

[14] www. Chemguide.co.uk.

[15] en.wikipedia.org.

[16] cnx.org

[16] T.K. Chaudhuri, A solar thermophotovoltaic converter using Pbs photovoltaic cells, Int. J. Energy Res. 16 (1992) 481.

[17] J.H. Dughaish, Lead telluride as a thermoelectric material for thermoelectric power generation, Physica B 322 (2002) 205.

[18] P.W. Bridgman, The Compression of 46 Substances to 50,000 kg/cm, Proc. Am. Acad. Sci.U.S.A.74 (1940) 21.

[19] T. Chattopadhyay, H.G.von Schnering, W.A. Grosshans, and W.B. Holzapfel, High pressure X-ray diffraction study on the structural phase transitions in PbS, PbSe and PbTe with synchrotron radiation,Physica 139 & 140B (1986) 356.

[20] K. Knorr, L. Ehm, B. Winkler, and W. Depmeier, The high-pressure α/β phase transition in lead sulphide (PbS), Eur. Phys. J. B 31 (2003) 297.

[21] S.V. Streltov, A Yu ManaKov, A.P. Vokhmyanin, S.V. Ovsyannikov and V.V. Shchennikov, Crystal lattice and band structure of the intermediate high-pressure phase of PbSe, J. Phys: Condense Matter 21 (2009) 385501.

[22] G. Rousse, S. Klotz, A.M. Saitta, J. Rodriguez-Carvajal, M.I. Mc. Mahon, B. Couzinet, and M. Mezouar, Structure of the intermediate phase of PbTe at high pressure, Phys. Rev. B 71 (2005) 224116.

[23] P. Toledano, K. Knorr, L. Ehm and W. Depmeier, Phenomenological theory of the reconstructive phase transition between the NaCl and CsCl structure types, Phys. Rev.B 67 (2003) 144106.

[24] V.V. Shchennikov, V. Ovsyannikov, A.Y. Manakov, A.Y. Likhacheva, A.I. Ancharov, I.F. Berger and M.A. Sheromov, Structure of the Intermediate HighPressure Phases of Ternary Lead Tellurides, JEPT Lett. 83 (2006) 228.

[25] J. Maclean, P.D. Hatton, R.O. Piltz, J. Crain and R.J. Cernik, Structural studies of semiconductors at very high pressures, Nucl. Instrum. Methods Phys. Res. B 97 (1995) 354.

[26] A.N. Mariano and K.L. Chopra, Polymorphism in some IV-VI compounds induced by high pressure and thin – film epitaxial growth, Applied Physics Letters 10 (1967) 282.

[27] Fan Da-Wei ZHOu Wen-Ge, WEI Shu-Yi, LIU Jing, LI Yan-Chun, JIANG Sheng and XIE Hong-Sen, Phase Relations and Pressure-Volume-Temperature Equation of State of Galena, CHIN. PHYS. LETT. 27 (2010) 086401.

[28] V. Sergey Ovsyannikov, V. Vladimir Shchennikov, E. Alexander Kar'kin and N. Boris Goshchitskii, High-pressure X-ray diffraction study of ternary and nonstoichiometric PbTe and PbSe crystals, J. Phys. Condens. Matter 17 (2005) 179.

[29] S.Yu. Ponosov, S.V. Ovsyannikov, S.V. Streltsov, V.V. Shchennikov and K. Syassen, Crystal lattice and band structure of the intermediate high-pressure phase of PbSe, High Pressure Res.29 (2009) 224.

[30] A. Grzechnik and K. Friese, Pressure-induced orthorhombic structure of PbS, J. Phys. Condens. Matter 22 (2010) 095402. [16] Y. Fujii, K. Kitamura, A. Onodera and Y. Yamada, A new high-pressure phase of PbTe above 16 GPa, Solid State Comm. 49 (1984) 135.